Deep-Sea Research I 93 (2014) 21–34

Contents lists available at ScienceDirect

Deep-Sea Research I

journal homepage: www.elsevier.com/locate/dsri

Development of the Western Boundary Undercurrent at Eirik Drift related to changing climate since the early Miocene

Antje Müller-Michaelis *, Gabriele Uenzelmann-Neben

Alfred-Wegener-Institut Helmholtz-Zentrum für Polar- und Meeresforschung, Am Alten Hafen 26, 27568 Bremerhaven, Germany

ARTICLE INFO

Article history:
Received 19 April 2013
Received in revised form
8 July 2014
Accepted 15 July 2014
Available online 30 July 2014

Keywords:
Sediment drift
Labrador Sea
North Atlantic Deep Water (NADW)
Western Boundary Undercurrent (WBUC)
North Atlantic thermohaline circulation (THC)
North Atlantic climate
Northern Hemisphere Glaciation
ODP Leg 105
IODP Expedition 303

ABSTRACT

Eirik Drift lies on the slope south of Greenland, where it has been formed under the influence of the Western Boundary Undercurrent (WBUC) closely downstream of its origin in the deep-water formation centres of the Nordic Seas. Therefore, the sediment record at Eirik Drift documents modifications in pathways and intensity of the WBUC. These modifications reflect alterations in deep-water formation in the Nordic Seas and are therefore coupled with climate changes. Based on the seismostratigraphic analysis of sedimentary architecture identified in a set of high-resolution seismic reflection data, we have reconstructed the palaeocirculation of the WBUC at Eirik Drift since the early Miocene. We revealed a strong WBUC during warm climate conditions, and in phases of climate cooling with enhanced sea-ice extent we interpreted weak WBUC influence. We suggest a southward shift of the deep-water formation regions along with a shift of the deep current system during the cool phases. This shift implies that the main North Atlantic Deep Water route affected Eirik Drift only during warm phases and that during cool phases weak branches of the circulation system flowed over Eirik Drift.

1. Introduction

Growing interest in climate research and coupled ocean–atmosphere interactions has led to numerous studies of the modern and ancient global ocean Thermohaline Circulation (THC), which is closely linked to the Earth's climate. Via the upper branch of the THC the surface ocean stores and transports heat and freshwater around the globe. The surface ocean interacts with the overlying atmosphere through surface fluxes of heat and freshwater (Schmitz, 1996; Van Aken, 2007). The compensating counterpart is the deep ocean circulation. The surface and the deep circulation are connected via deep-water formation in high latitudes and Southern Ocean upwelling (Marshall and Speer, 2012). North Atlantic Deep Water (NADW) formation is the main driving mechanism for the North Atlantic branch of the THC (Dickson and Brown, 1994; Schmitz, 1996; Van Aken, 2007). Thus, NADW production and circulation is of highest importance for the global THC and the global climate (Dickson and Brown, 1994; Schmitz, 1996). Here, we contribute to the understanding of the development of this complex interplay by investigating changes in the deep circulation of the northern North Atlantic Ocean, closely downstream of the present NADW formation region. From their formation regions in the Nordic Seas the NADW components meet southeast of Greenland and combine to form the Western Boundary Undercurrent (WBUC; Fig. 1). Eirik Drift south of Greenland is a sediment drift lying directly under the pathway of the present WBUC (Arthur et al., 1989; Hunter et al., 2007a; Müller-Michaelis et al., 2013; Wold, 1994). Here, we investigate the sedimentary architecture of Eirik Drift to better understand the development of the ancient WBUC.

We have analysed high-resolution multichannel seismic reflection data at Eirik Drift, gathered in 2009, combined with geological information from four ODP/IODP sites. In this study, we focus on a detailed reconstruction of interface outlines and depocentre geometries of Eirik Drift. The location and orientation of the depocentres and their interface outlines allow us to develop a conceptual model of the palaeocurrents in the vicinity of Eirik Drift. Changes in pathways and strength of the palaeocirculation are discussed with respect to changes in climate.

2. Background and settings

2.1. Oceanographic setting

The global THC is driven by deep-water formation in high latitudes due to thermohaline convection and by Southern Ocean

* Corresponding author.
E-mail address: Antje.Mueller-Michaelis@awi.de (A. Müller-Michaelis).

http://dx.doi.org/10.1016/j.dsr.2014.07.010
0967-0637/

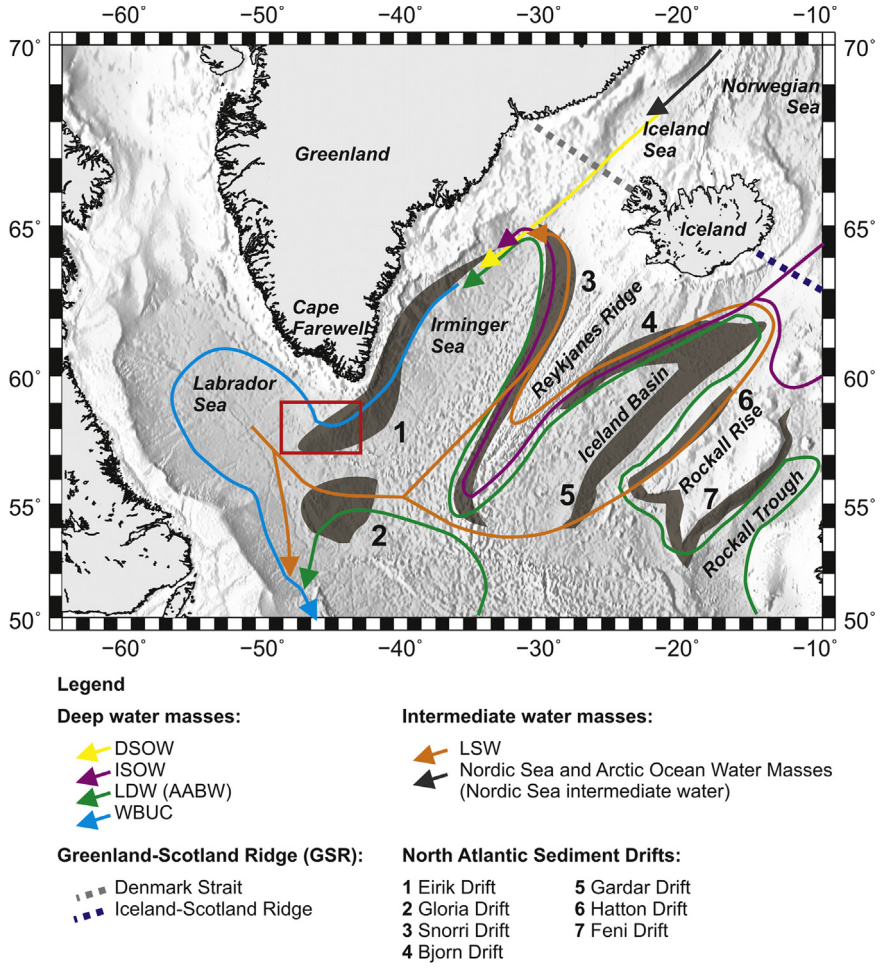

Fig. 1. Satellite bathymetry map (Smith and Sandwell, (1997)) including basins, ridges, sediment drifts and prevailing deep-current system of the North Atlantic Ocean (modified from Müller-Michaelis et al., (2013); sediment drifts after Faugères et al., (1999)). The present Western Boundary Undercurrent (WBUC) at Eirik Drift transports Denmark Strait Overflow Water (DSOW), Iceland–Scotland Overflow Water (ISOW), Lower Deep Water (LDW; also: modified Antarctic Bottom Water AABW) and Labrador Sea Water (LSW) (modified from Schmitz, 1996). Red box shows the study area (see Fig. 2).

upwelling (Marshall and Speer, 2012). Present deep-water formation is conducted in a bipolar mode in the polar regions of both the Northern and Southern Hemisphere (Van Aken, 2007). On the Southern Hemisphere shelf ice convection is dominant and forms the densest water mass, Antarctic Bottom Water (AABW). AABW is modified by entrainment on its way north and this modified AABW is also referred to as Lower Deep Water (LDW) (Marshall and Speer, 2012; Van Aken, 2007). On the Northern Hemisphere the open ocean convection due to atmospheric cooling prevails. Open ocean convection produces NADW, which is the main driver of the North Atlantic part of the THC (Dickson and Brown, 1994; Schmitz, 1996). The deep-water formation regions on the Northern Hemisphere comprise the Nordic Seas, i.e. the Greenland Sea and the Norwegian Sea, and the Labrador Sea (Fig. 1) (Kuhlbrodt et al., 2007; Quadfasel and Käse, 2007). In these regions, sufficient atmospheric cooling and cyclonic surface ocean gyres allow convective mixing to greater depths of the deep basins. The deep-water formed in the Norwegian and Greenland Sea spills over the Greenland–Scotland-Ridge (GSR) as dense overflows (Fig. 1) (Quadfasel and Käse, 2007; Van Aken, 2007). The overflows recirculate around the Irminger and Labrador basins and entrain different amounts of ambient water, mainly Labrador Sea Water (LSW) formed by open ocean convection in Labrador Sea, but also warm NE Atlantic water and LDW (Fig. 1) (Quadfasel and Käse, 2007; Smethie and Fine, 2001). LSW, Iceland Scotland Overflow Water (ISOW), Denmark Strait Overflow Water (DSOW) and LDW meet at the southeast coast of Greenland. Here, they combine to form the North Atlantic Western Boundary Undercurrent (WBUC), a complex flow system of overlying water masses of different densities, which flows equatorward along the western continental slope (Dickson and Brown, 1994; Schmitz, 1996). In the vicinity of Eirik Drift the WBUC comprises LSW in water depths of 700 to 2500 m, ISOW between 2500 and 3500 m, and DSOW beneath 3500 m (Pickart, 1992). In regions of complex topography, especially at a margin corner like Cape Farewell, this flow might split up into different strands following different depth contours according to the core density of the transported water mass of the WBUC. The deep water, which was formed in the Nordic Seas and northern North Atlantic Ocean in former times, differs in composition from the modern NADW due to changing tectonic and climatic conditions. Deep water produced in the Nordic Seas prior to the modern NADW is therefore referred to as Northern Component Water (NCW).

2.2. Geological background

The Labrador Sea was formed by rifting between Greenland and Labrador during the Late Cretaceous (Chalmers and Pulvertaft, 2001; Srivastava and Arthur, 1989). Active sea-floor spreading ceased ~35 Ma ago (Srivastava and Roest, 1999). Approximately

at the same time (~35–33 Ma) the bipolar mode of the THC with the onset of deep-water formation in the Nordic Seas established (Via and Thomas, 2006). The cause for the distribution of NCW is presumably the subsidence of the Greenland–Scotland-Ridge (GSR; Fig. 1) (Via and Thomas, 2006). This is the topographic barrier between the Nordic Seas and the northern North Atlantic Ocean. The western part of the GSR between Iceland and Greenland is called Denmark Strait with a present sill depth of ~600 m (Fig. 1) (Wright and Miller, 1996). The eastern part of the GSR is the Iceland–Scotland-Ridge (Fig. 1). The Iceland–Faroe-Ridge with an actual sill depth of ~400 m forms the western part of the Iceland–Scotland-Ridge (Wright and Miller, 1996). At the eastern part of the Iceland–Scotland-Ridge the Faroe–Shetland-Channel forms the deepest part of the GSR with ~1000 m depth. The Faroe–Shetland-Channel is connected to the Irminger Basin of the northern North Atlantic Ocean through the N–S orientated Faroe-Bank-Channel at ~800–1000 m depth (Stoker et al., 2005). Towards the south to the Rockall Trough region the Faroe–Shetland-Channel ceases at the Wyville-Thomson-Ridge with a present sill depth of ~500 m.

2.3. Contourite drifts

Contour currents are thermohaline-driven and received their names as they roughly follow the same depth contours, which are congruent with their density level within the stratified ocean (Heezen et al., 1966). The concentrated and intensified flow of the current core accounts for non-deposition and/or erosion of sediments at the current core depth (e.g. Stow et al., 2008). The eroded and transported sediment within the current is transported to and re-deposited on the tranquil sides. Deposition is always to the right for detached elongated mounded drifts like Eirik Drift on the Northern Hemisphere (e.g. Faugères et al., 1999). The depocentres are distributed along-slope at certain depth contours and are of lenticular or sigmoidal shape. Their bedding thickens at the drift axis with diverging internal reflections and thins at their drift flanks with converging internal reflections (e.g. Nielsen et al., 2008). These thin parts represent the erosional centres, i.e. the locations of the contour current core (e.g. Faugères and Stow, 2008). If the current core was particularly strong, also reflector truncation could be observed at the erosional centre (e.g. Nielsen et al., 2008). Within identified contourite deposits the amplitudes of the internal seismic reflections can give additional information about the strength of the deep current regime. Increasing amplitudes of internal reflections can indicate an intensification of deep current activity as long as the composition of supplied sediment does not change. With a stable composition of sediments the increasing amplitudes must result of changes in grain sizes, which yield modifications in impedance contrast (Stow et al., 2002).

2.4. Seismostratigraphy

High-resolution seismic reflection data gathered in 2009 with RV Maria S. Merian, which were correlated with synthetic seismograms for drill sites ODP Leg 105 Site 646 (ODP 646) and IODP Expedition 303 Sites U1305-U1307 (IODP 1305-1307), form the basis of this study (Fig. 2). Data processing and the correlation of the age model of ODP Site 646 (Arthur et al., 1989) to the seismic data are described in detail in Müller-Michaelis et al. (2013). The revised seismostratigraphic concept for Eirik Drift and the detailed investigation of seismic unit SUIV are only briefly described here in order not to repeat the detailed discussion presented there. The following paragraph is the essence of Müller-Michaelis et al. (2013) unless otherwise cited. Four different units were defined, while prominent internal reflection horizons subdivide some of these (Figs. 3–5). The irregular seismic basement (60–40 Ma; Figs. 3–5) is overlain by unit SUIV. Unit SUIV comprises the period 40–8.1 Ma and is subdivided into subunits SUIV-c (40–19 Ma), SUIV-b (17–12 Ma) and SUIV-a (10–8.1 Ma) (Figs. 3–5). Subunit SUIV-c is almost acoustically transparent and is interpreted to represent an infill and drape of the irregular basement topography in an environment not controlled by deep currents (Figs. 3–5). The top horizon A3 (19–17 Ma) of subunit SUIV-c is identified as the basal erosional unconformity of Eirik Drift. The deposition of subunit SUIV-b documents the onset of drift building under the influence of strong NCW fluxes, which were inhibited between 15 and 12.5 Ma. A renewed onset of strong NCW flow formed horizon R5 (12–10 Ma), which separates subunits SUIV-b and SUIV-a. The top reflector doublet R3/R4 (8.1/7.5 Ma) and the medium- to high amplitude reflections found below this horizon are ascribed to minor interruptions of NCW flow at 7 and 9 Ma. It is suggested that horizon R3 documents the onset of DSOW flow.

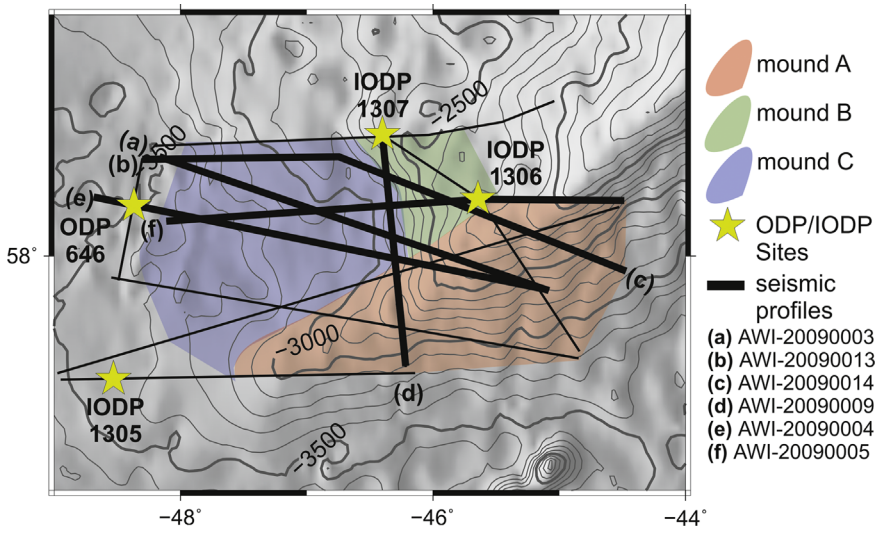

Fig. 2. Satellite bathymetry map (Smith and Sandwell (1997); red box in Fig. 1) modified from Müller-Michaelis et al. (2013) showing the location of the seismic lines (black lines). Bold seismic lines are displayed in Fig. 3 (AWI-20090003 (a)), Fig. 4 (AWI-20090013 (b) and AWI-20090014 (c)), and Fig. 5 (AWI-20090009), and in Müller-Michaelis et al. (2013) (20090004 (e) and 20090005 (f)). Yellow stars show ODP Leg 105 Site 646 (Shipboard Scientific Party, 1987) and IODP Expedition 303 Sites U1305, U1306 and U1307 (Channell et al., 2010). Mound A is marked red, mound B green, and mound C blue.

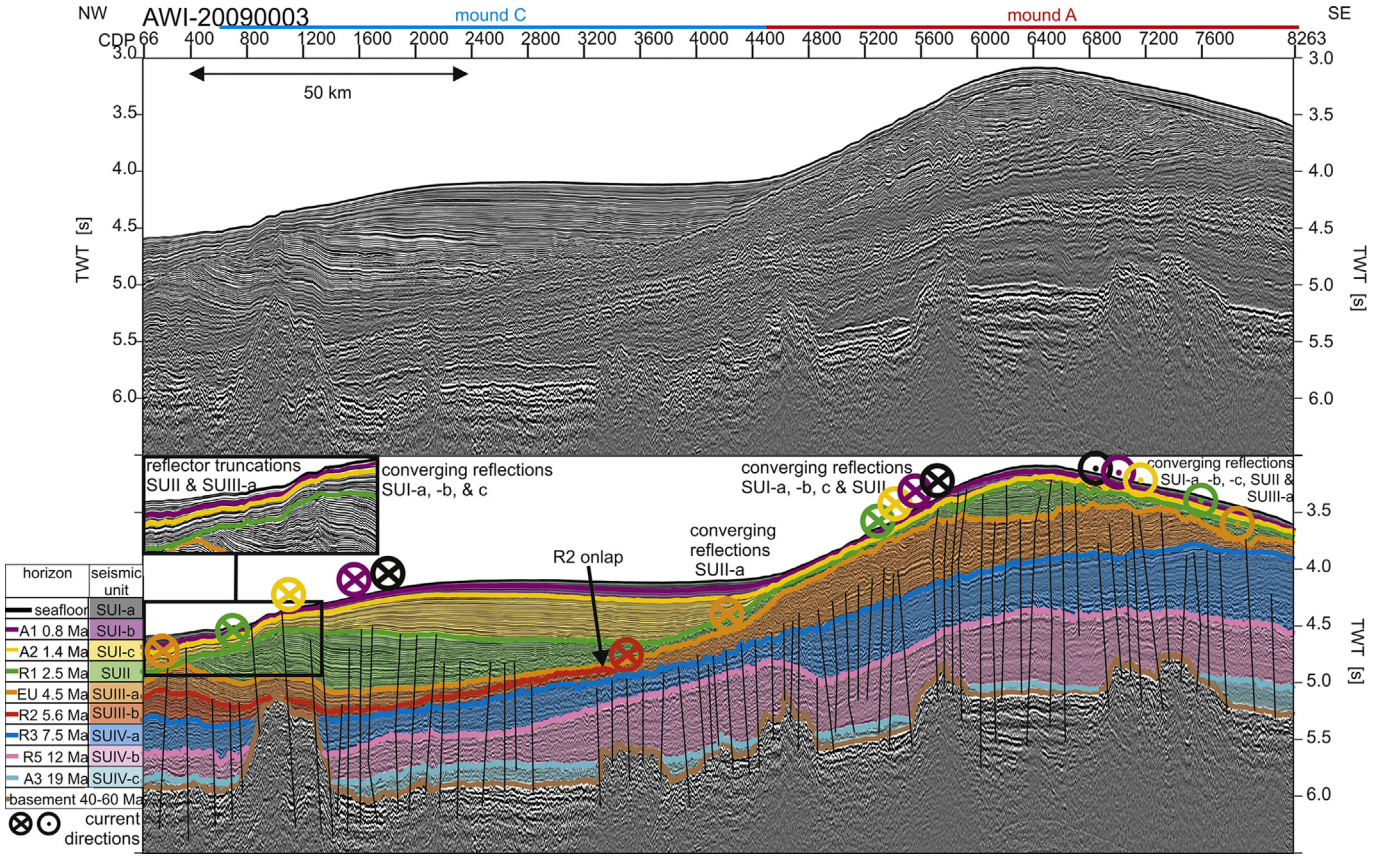

Fig. 3. Uninterpreted (top) and interpreted (bottom) line AWI-20090003. For location see Fig. 2. Horizons: A1 (magenta; 0.8 Ma), A2 (yellow; 1.4 Ma), R1 (green; 2.5 Ma), erosional unconformity EU (orange; 4.5 Ma), R2 (red; 5.6 Ma), reflection doublet R3/R4 (blue; 7.5/8.1 Ma), R5 (pink; 10–12 Ma), A3 (cyan; 17–19 Ma) and basement (brown; ~40–60 Ma). Circles in the colour of the top-horizon indicate the interpreted location of the current core and its direction for the respective seismic sub-unit. Inset shows reflector truncations.

Unit SUIII extends from horizon doublet R3/R4 (8.1/7.5 Ma) to the erosional unconformity EU (4.5 Ma) and is subdivided by the internal medium-amplitude horizon R2 (5.6 Ma). Unit SUIII comprises narrowly spaced, parallel to subparallel low amplitude reflections in the lower part (subunit SUIII-b, 7.5–5.6 Ma) and an increase in amplitudes and reflection spacing in the upper part (subunit SUIII-a, 5.6–4.5 Ma; Figs. 3–5).

Unit SUII (4.5–2.5 Ma) is characterized by narrowly-spaced, continuous high-amplitude reflections (Figs. 3–5). Reflector truncations are observed at unit SUII's top horizon R1 (2.5 Ma; Figs. 3–5). These reflector truncations indicate an intense NCW flow. Furthermore, horizon R1 marks the onset of Northern Hemisphere Glaciation and major ice rafting at Eirik Drift (Arthur et al., 1989).

The youngest unit SUI (2.5–0 Ma) is subdivided into subunits SUI-c (2.5–1.4 Ma), SUI-b (1.4–0.8 Ma) and SUI-a (0.8–0 Ma) by the internal horizons A2 (1.4 Ma) and A1 (0.8 Ma) (Figs. 3–5). Within subunit SUI-c wide-spaced, continuous to discontinuous, parallel to subparallel internal reflections are observed, which increase in amplitude towards the top horizon A2 (Figs. 3–5). Subunit SUI-b comprises continuous to discontinuous, narrowly-spaced, parallel medium-amplitude reflections, while SUI-a is characterized by continuous, parallel to subparallel high-amplitude reflections (Figs. 3–5). No reflector truncation is observed (Figs. 3–5). There is a major change in the sediment lithology at 2.5 Ma and a minor change within unit SUI (Cremer et al., 1989). Therefore, the high-amplitude internal reflections may be related to lithology and could not be used for the interpretation of the deep current intensity.

3. Methods

For this study of the development of the WBUC we applied the seismostratigraphic concept of Müller-Michaelis et al. (2013) and tracked the seismic horizons. Please note that our grid of seismic reflection data is not uniform (Fig. 2). The resulting maps (Figs. 6 and 7) therefore are afflicted with uncertainties in the uncovered areas, but the overall trend of interface outlines and distribution and re-localisation of the depocentres is probably correct.

We calculated the depth of each seismic horizon, which results in the interface outlines (Fig. 6a, c, e and g) and the thicknesses of each seismic unit (Fig. 6b, d, f and h). Values greater than the root mean square (rms) value of each horizon's depth are defined to represent topographic highs of the interface outlines (Fig. 6a, c, e and g). Consistently, depocentres of each seismic unit are defined by values greater than the rms value of the unit's thickness (Fig. 6b, d, f and h). Thus, we gain a detailed image of interface outlines and depocentre geometries of each seismic unit in the study area and the distribution and location of topographic highs and lows of the interface outlines as well as of the depocentres of each seismic unit are mapped (Fig. 6). Orientation and location of the depocentres are interpreted in relation to the morphology of the underlying horizon. Depocentres parallel to the slope of the basal horizons are interpreted as a result of along-slope sediment transport, i.e. contour current controlled deposition. Stronger flow of a contour current causes erosion and/or reduced net accumulation, while sediment accumulates in the comparatively tranquil zones to the right (in the Northern Hemisphere) of the current

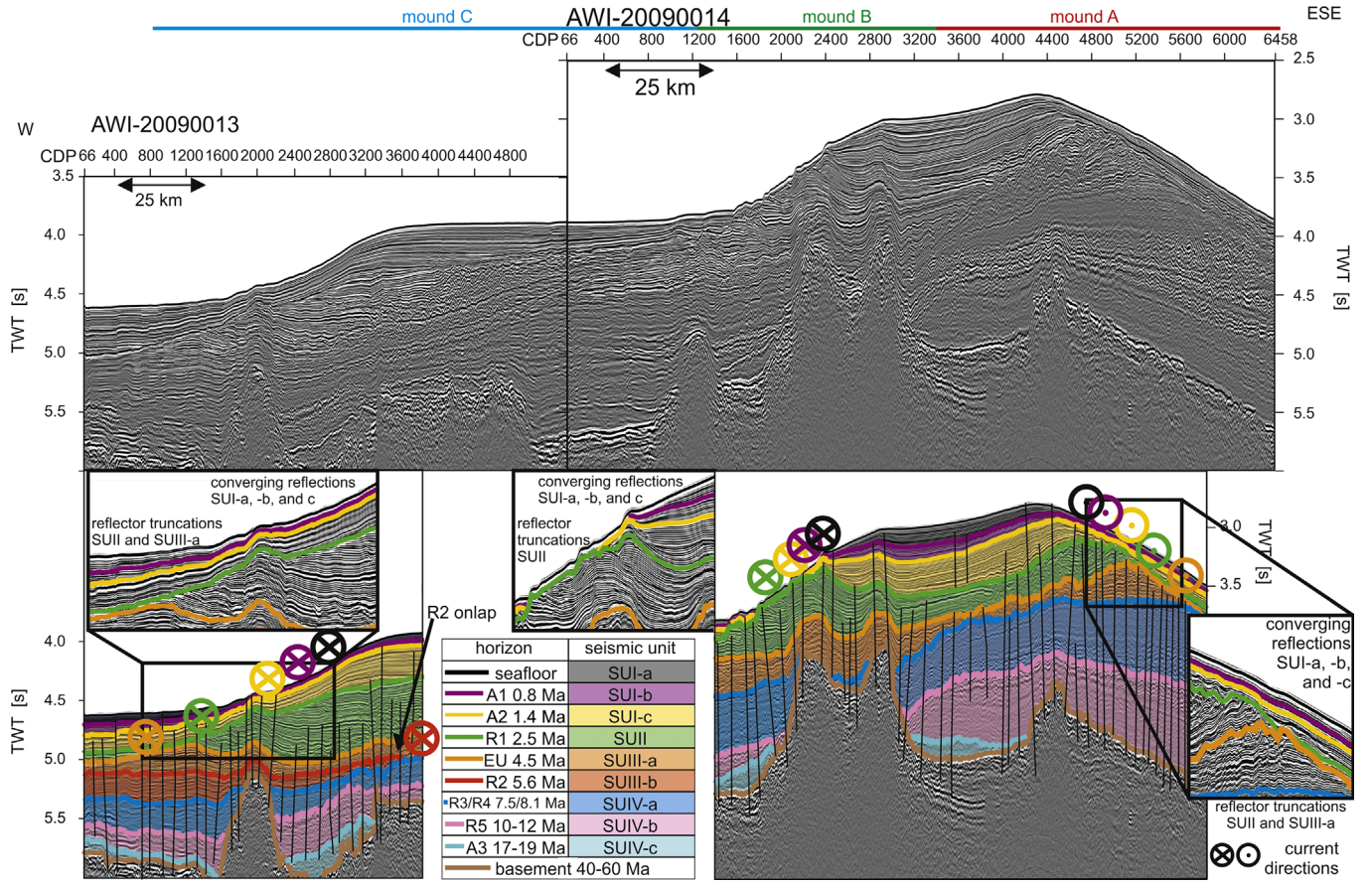

Fig. 4. Uninterpreted (top) and interpreted lines AWI-20090013 and AWI-20090014. For location see Fig. 2. Horizons: A1 (magenta; 0.8 Ma), A2 (yellow; 1.4 Ma), R1 (green; 2.5 Ma), erosional unconformity EU (orange; 4.5 Ma), R2 (red; 5.6 Ma), reflection doublet R3/R4 (blue; 7.5/8.1 Ma), R5 (pink; 10–12 Ma), A3 (cyan; 17–19 Ma) and basement (brown; 40–60 Ma). Circles in the colour of the top-horizon indicate the interpreted location of the current core and its direction for the respective seismic sub-unit. Insets show reflector truncations and converging reflections.

core (e.g. Faugères and Stow, 2008). Therefore, the thin parts of each seismic (sub)unit can be interpreted as the erosional centres, which indicate the location of the prevailing deep current core in each time interval. The internal reflection characteristics of each seismic line help to support this interpretation when converging internal reflections or even reflector truncation are found at the erosional centres (see Section 2.4; as examples Figs. 3–5). The interpretation of the deep current core location for each subunit was transferred to the contour plots of their basal horizons (Fig. 7). Additionally, the locations of the depocentres of each seismic subunit were marked (Figs. 6 and 7), which we expect to the right of the erosional centres (Faugères and Stow, 2008), and thus we are able to estimate the deep current direction. This interpretation of deep current development at Eirik Drift was correlated with information of other North Atlantic Drifts and tectonic changes in this region to develop a conceptual deep circulation model of the northern North Atlantic Ocean (Fig. 8).

A palaeo-bathymetric grid of the northern Northeast Atlantic with a grid cell size of $1^\circ \times 1^\circ$ and a temporal resolution of 5 Ma (Ehlers and Jokat, 2013) was used to support our interpretation (Fig. 8). Unfortunately, the available grids cover only parts of our investigation area (Fig. 8).

4. Results

First, we describe the present seafloor morphology of Eirik Drift, then describe the (sub)units and their bounding horizons from bottom to top, i.e. from the oldest to the youngest, starting with the seismic basement.

4.1. Seafloor

The seafloor is characterised by three mounds (Fig. 2). Mound A forms an elongated, ridge-like structure, which extends from the NE to the SW (Fig. 2). In the NE mound B extends almost perpendicular to mound A's crest to the NW (Fig. 2). Adjacent to mound A and B, mound C slopes to the west (Fig. 2).

4.2. Basement

The seismic basement is an irregular, hummocky high amplitude reflection, which marks the top of the oceanic crust (as examples Figs. 3–5; Müller-Michaelis et al., 2013). The basement shows a high in the NE and the deepest part of the horizon can be observed in the west (Fig. 6a; Müller-Michaelis et al., 2013). Several basement highs are found at mound A (Figs. 3–5 and Fig. 6a) and form the axes of the southern WSW-trending basement ridge (Fig. 6a) (Le Pichon et al., 1971; Müller-Michaelis et al., 2013; Srivastava and Arthur, 1989). A second WSW-trending basement ridge north of and parallel to the latter (Le Pichon et al., 1971; Srivastava and Arthur, 1989) is found below mound B (Figs. 4 and 6a; Müller-Michaelis et al., 2013). Additional basement elevations are found in the NW at mound C (Figs. 3–5 and Fig. 6a) (Uenzelmann-Neben et al., 2012; Müller-Michaelis et al., 2013).

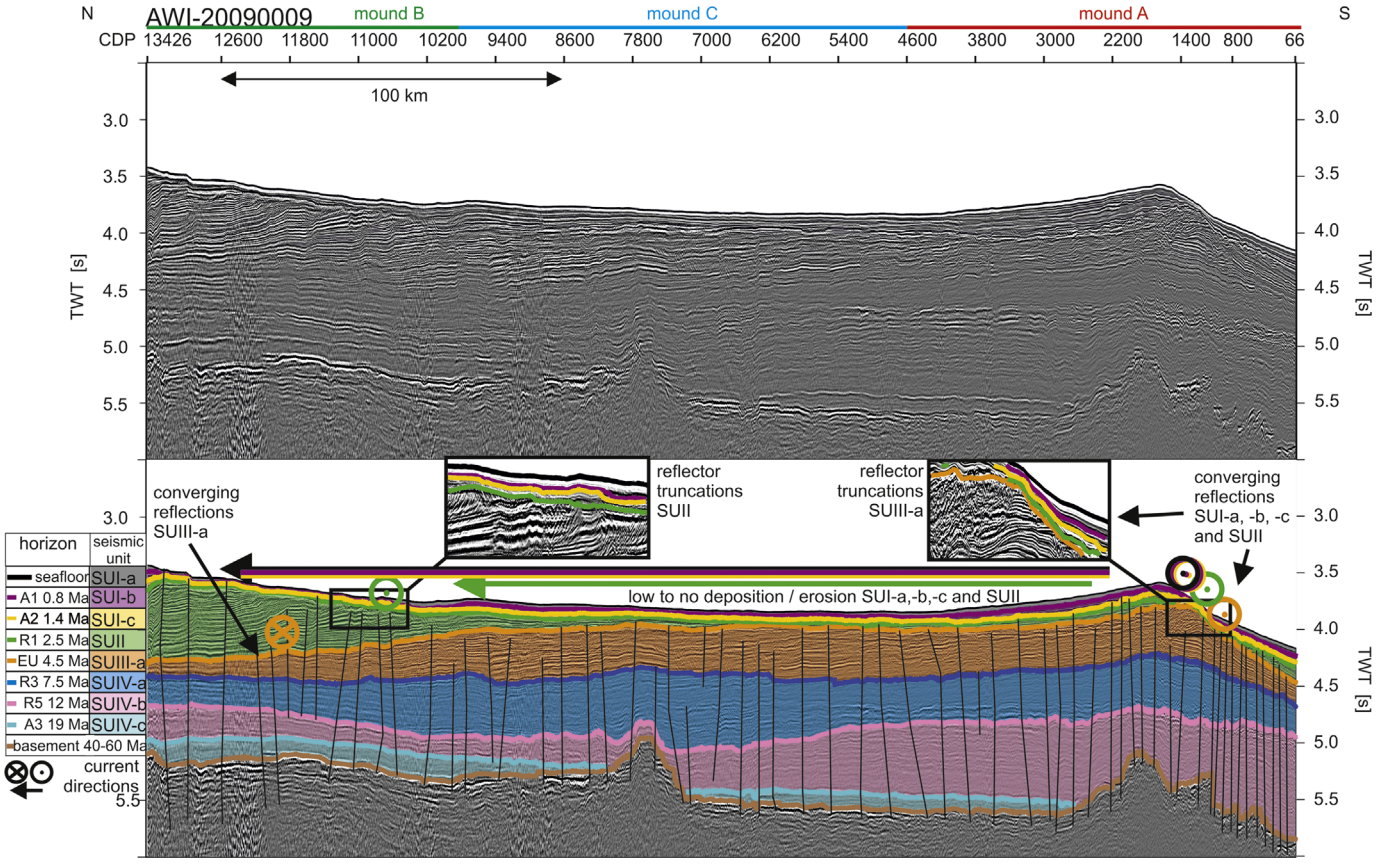

Fig. 5. Uninterpreted (top) and interpreted (bottom) line AWI-20090009. For location see Fig. 2. Horizons: A1 (magenta; 0.8 Ma), A2 (yellow; 1.4 Ma), R1 (green; 2.5 Ma), erosional unconformity EU (orange; 4.5 Ma, reflection doublet R3/R4 (blue; 7.5/8.1 Ma), R5 (pink; 10–12 Ma), A3 (cyan; 17–19 Ma) and basement (brown; 40–60 Ma). Circles and arrows in the colour of the top-horizon indicate interpreted location of the current core and its direction for the respective seismic sub-unit. Insets show reflector truncations.

4.3. Unit SUIV

The main part of the depocentre of unit SUIV (> 863 ms TWT) is found in the SE (Fig. 6b; Müller-Michaelis et al., 2013). This depocentre surrounds the NE basement high (Fig. 6a and b; Müller-Michaelis et al., 2013). In subunit SUIV-c several small depocentres infill the basement topography and thus lead to a smoothed morphology of horizon A3 compared to the underlying basement horizon. In the overlying subunits SUIV-b and SUIV-a a distinct depocentre is observed in the SE (Müller-Michaelis et al., 2013). This depocentre encloses the NE topographic high of the basal horizons and shows a winding western boundary (Müller-Michaelis et al., 2013). The depocentre of subunit SUIV-b extends farther to the south than that of subunit SUIV-a (Müller-Michaelis et al., 2013). The bulges observed at the western boundary of the depocentre are more pronounced in subunit SUIV-a than in subunit SUIV-b (Müller-Michaelis et al., 2013).

4.4. Unit SUIII

In contrast to unit SUIV (Fig. 6b) the main depocentre of unit SUIII (> 376 ms TWT) is observed in the SW (Fig. 6d). This depocentre lies mainly in the topographic low of horizon R3/R4 at mound C (Fig. 6c and d). Smaller depocentres are found aligned along the western flank of the topographic high of horizon R3/R4 (Fig. 6c and d), which correspond to the western flanks of mound A and mound B. Subunit SUIII-b thins from 300 ms TWT in the SW to 0 ms TWT in the E where horizon R2 onlaps horizon R3/R4 (Figs. 3 and 4). The depocentre of subunit SUIII-b is SW-NNE orientated. In subunit SUIII-a the depocentre shifts towards the E. The smaller depocentres observed along the western flanks of mound A and mound B (Fig. 6d) belong to subunit SUIII-a.

4.5. Unit SUII

In unit SUII the depocentres (> 226 ms TWT) shifted to the N (Fig. 6f). Two connected main depocentres are observed (Fig. 6f). The western part infills the eastern topographic low of horizon EU (Fig. 6e and f). The eastern part overlies the topographic high of horizon EU at mound A and mound B (Fig. 6e and f). The connection of western and eastern part of the depocentre thins at the boundary between the topographic highstand and lowstand of the basal horizon EU (Fig. 6f). Here, the sediment thickness just slightly exceeds the rms value of 226 ms TWT (Fig. 6f) and the internal reflections converge. In the south and in the very east unit SUII is characterized by a thin cover (Figs. 3–5 and Fig. 6f).

4.6. Unit SUI

In unit SUI we observe the separation of the two parts of the depocentre (> 274 ms TWT; Fig. 6h). The western depocentre at mound C fills the eastern topographic low of horizon R1 (Fig. 6g and h). This western depocentre has shifted to the south (Fig. 6f and h). The eastern depocentre remains in the NE on top of the topographic high of the basal horizon R1 at mound A and mound B (Fig. 6g and h). The thinnest part of unit SUI surrounds this NE depocentre. Within the subunits SUI-c, SUI-b and SUI-a the western depocentre at mound C (Fig. 6h) is shifted gradually to the south following the changing morphology of the basal horizons.

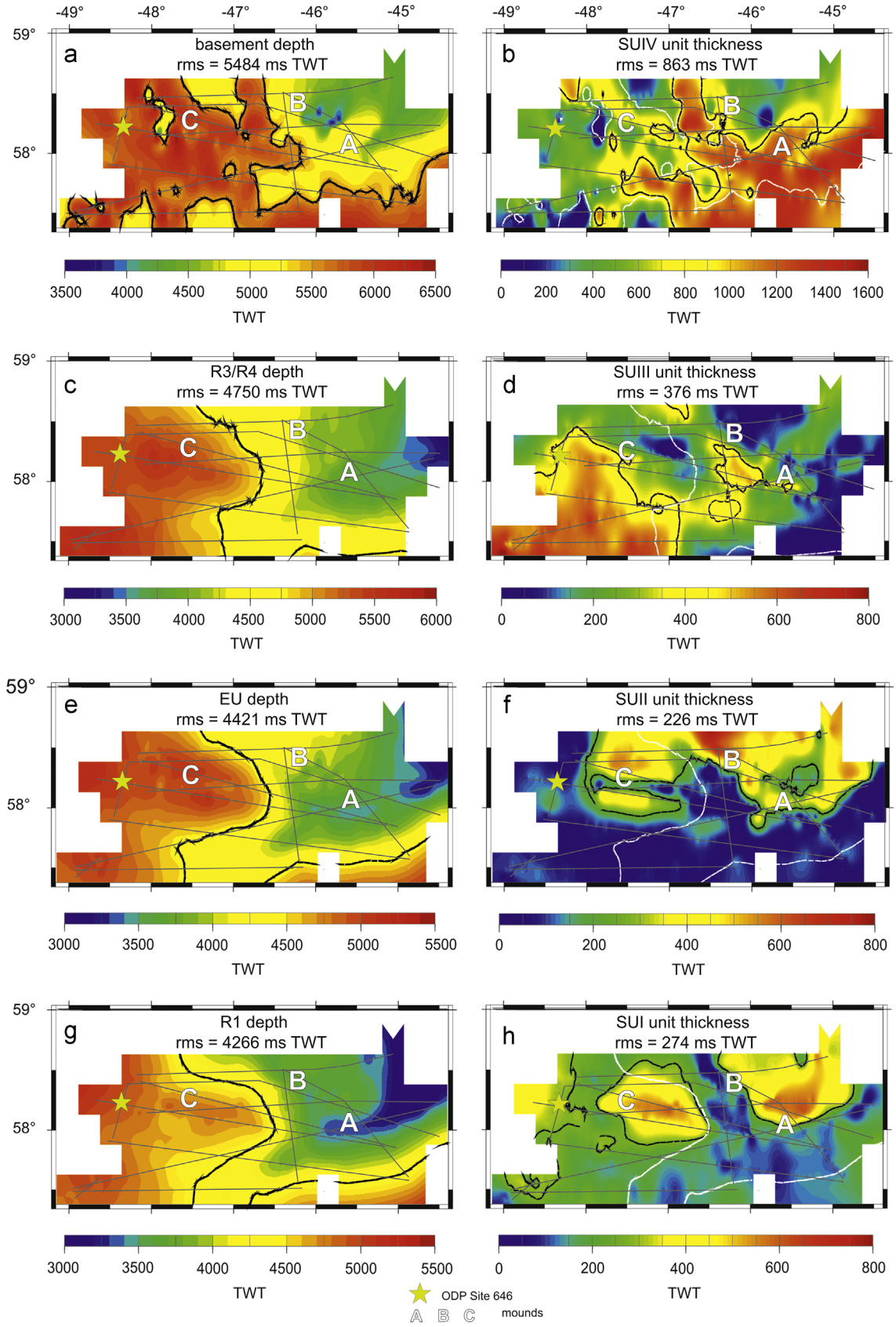

Fig. 6. Contour maps of horizon depth ((a), (c), (e) and (g)) and unit thickness ((b), (d), (f) and (h)). Grey lines show the locations of the seismic profiles. Black lines indicate the root mean square (rms) depth ((a), (c), (e) and (g)) and rms thickness ((b), (d), (f) and (h)), respectively. RMS depth outline of the topographic high of the basal horizon is added in unit thickness plots ((b), (d), (f) and (h)) as white lines. Locations of mounds A, B and C are indicated by white letters. (a) basement depth (from Müller-Michaelis et al. (2013)); (b) unit SUIV thickness, white line: basement topographic high outline (from Müller-Michaelis et al. (2013)); (c) horizon R3/R4 depth (from Müller-Michaelis et al. (2013)); (d) unit SUIII thickness, white line: R3/R4 topographic high outline; (e) horizon EU depth; (f) unit SUII thickness, white line: EU topographic high outline; (g) horizon R1 depth; (h) unit SUI thickness, white line: R1 topographic high outline.

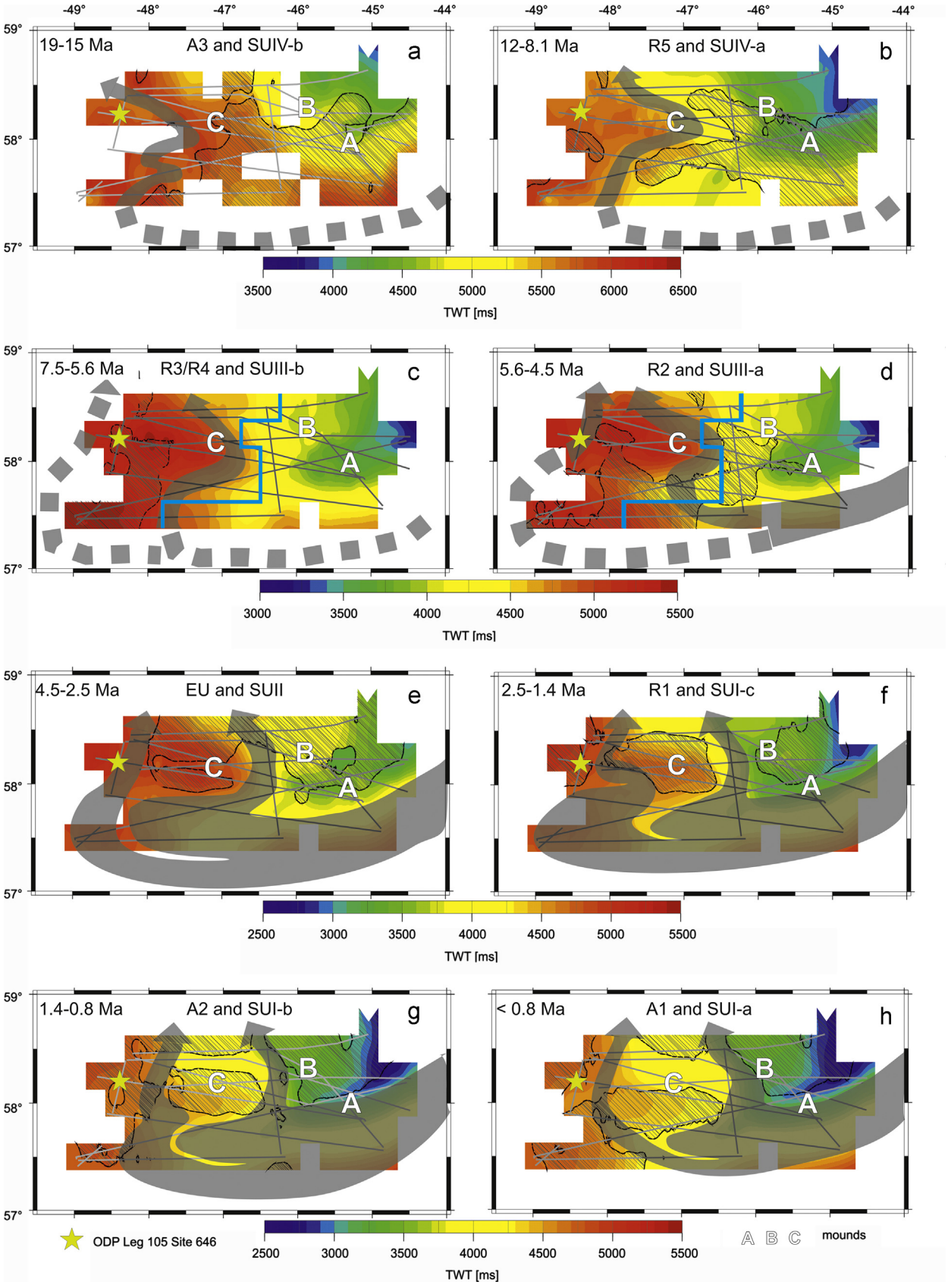
-49°
-48°
-47°
-46°
-45°
-44°
59°
58°
57°
19-15 Ma
A3 and SUIV-b
a
12-8.1 Ma
R5 and SUIV-a
b
7.5-5.6 Ma
R3/R4 and SUIII-b
c
5.6-4.5 Ma
R2 and SUIII-a
d
4.5-2.5 Ma
EU and SUII
e
2.5-1.4 Ma
R1 and SUI-c
f
1.4-0.8 Ma
A2 and SUI-b
g
< 0.8 Ma
A1 and SUI-a
h
A
B
C
3500 4000 4500 5000 5500 6000 6500
3000 3500 4000 4500 5000 5500
2500 3000 3500 4000 4500 5000 5500
TWT [ms]
ODP Leg 105 Site 646
A B C mounds

5. Discussion

Eirik Drift has been built under the influence of varying deep currents since the formation of the basal unconformity A3 (~19–17 Ma) (Müller-Michaelis et al., 2013). The distinct depocentres within each seismic unit after the formation of the basal unconformity A3 are found alongslope, i.e. within certain depth contours of the underlying horizons (Fig. 6b, d, f and h). This supports the interpretation of current controlled sedimentation since then (Uenzelmann-Neben, 2001; Uenzelmann-Neben and Gohl, 2012; Uenzelmann-Neben and Huhn, 2009; Uenzelmann-Neben et al., 2007). The shapes and locations of these depocentres shift from one unit to the next (Fig. 6b, d, f and h). These shifts along with changes in the internal structure and reflection characteristics reflect changes in the prevailing contour current flow in each time interval. By identifying the locations of the erosional and depositional centres in combination with the basal interface outlines (Fig. 6) a conceptual model for the development of the deep palaeocurrents at Eirik Drift is assessed (Fig. 7). This conceptual model provides the basis for the discussion of a possible interplay of oceanographic, climatic and tectonic conditions in the northern North Atlantic (Fig. 8).

5.1. Unit SUIV (> 7.5 Ma)

The depocentres of subunits SUIV-b (~17–15 Ma; Fig. 7a) and SUIV-a (~12–8.1 Ma; Fig. 7b) are found in the SE of the study area, surrounding the topographic high of their basal horizons in the NE (Fig. 6b, Fig. 7a and b; Müller-Michaelis et al., 2013). The erosional centres, i.e. the interpreted locations of the deep current core, follow a certain depth contour in the western part of the study area (Fig. 7a and b; Müller-Michaelis et al., 2013). The locations of erosional and depositional centres as well as the morphology of the basal horizons suggest a W–E winding, northward-directed flow in the western part of the study area before it turns to the NE (Fig. 7a and b). The depositions and therefore also the suggested NCW flow shallowed and shifted to the E from subunit SUIV-b (Fig. 7a) to subunit SUIV-a (Fig. 7b) and the bulges at the western flank of the depocentre are more pronounced. The suggested winding NCW flow at the western flank of the depocentre is therefore also more winding within subunit SUIV-a (Fig. 7b), which might be caused by an intensified NCW flow with enhanced erosion. This is in accordance to Müller-Michaelis et al. (2013) who suggested that the high-amplitude reflection band surrounding basal horizon R5 represents a renewed onset and a change in the deep current system at 12–10 Ma. Our study area does not cover the full spatial extent of the depocentres to the S and E (Fig. 7a and b). However, the slope of the basal horizons from NE to SW and the orientation of the depocentres along this slope suggest a WSW directed flow at the SE flank of mound A outside the study area, before it turns to the inferred northern direction (Fig. 7a and b).

The GSR has been the limiting factor for the overflows of NCW into the North Atlantic Ocean before early Oligocene (Via and Thomas, 2006). Sufficient subsidence of the GSR and NCW overflow at the distal eastern part is determined to have occurred at the early Oligocene (Wright and Miller, 1996). Davies et al. (2001) suggested the onset of NCW overflow into the Rockall Trough region at ~35–33 Ma with a southward directed flow (Fig. 8a). This southward-directed NCW flow is documented in the Feni Drift (Fig. 8a) with a stable drift accumulation since ~34 Ma (Miller et al., 2009; Wold, 1994; Wright and Miller, 1996). This early, southward directed NCW flow during the cold Oligocene climate does not appear to have affected Eirik Drift or any other North Atlantic drift besides Feni Drift (Fig. 8a). Presumably due to the cold climate the NCW was denser and therefore flowing at a deeper depth contour towards the south instead of recirculating around the northern North Atlantic Ocean towards the west.

The onset of strong NCW fluxes at ~19–17 Ma (Wright and Miller, 1996) was suggested not only for horizon A3 at Eirik Drift (Müller-Michaelis et al., 2013) but is also documented in a widespread erosional unconformity in the northern North Atlantic Ocean (Miller and Tucholke, 1983; van Weering et al., 2008; Wold, 1994). Stoker et al. (2005) suggested that the Faroe Conduit developed in early Miocene and formed the first true deep-water connection between the Atlantic Ocean and the Nordic Seas. The early Miocene NCW overflow over the eastern part of the Iceland–Scotland-Ridge and the resulting NCW deep circulation is documented in the onset of drift building within the Iceland Basin at Bjorn and Gardar Drift but not traceable at drifts within the Irminger Sea (Fig. 8b). We therefore suggest a NCW flow between 19 and 15 Ma as depicted in Fig. 8b with presumably no overflow at the still shallow Denmark Strait as shown in the palaeobathymetry (Ehlers and Jokat, 2013) and such an overflow should have resulted in drift accumulation in the Irminger Sea (Fig. 8b). The first indications for strong NCW flow at Eirik Drift (~19–15 Ma) and in the northern North Atlantic Ocean are interpreted for the Mid Miocene Climate Optimum (~20–15 Ma).

Low to no NCW flux in the North Atlantic Ocean has been suggested between 16 and 12.5 Ma (Woodruff and Savin, 1989; Wright et al., 1992) and also at Eirik Drift at 15–12.5 Ma (Müller-Michaelis et al., 2013). This coincides with the cooling during the Mid Miocene Climate Transition (Zachos et al., 2001). Presumably, this cooling accounted for the production of NCW with increased density and additionally, the GSR was still too shallow to allow a significant overflow (Ehlers and Jokat, 2013; Poore et al., 2006; Wright, 1998). The renewed onset of strong deep current activity at Eirik Drift at ~12 Ma follows the cooling of the mid Miocene Climate Transition along with the ongoing submergence of Iceland–Faroe Ridge caused by lithospheric plate cooling (Poore et al., 2006; Wright, 1998). A renewed onset of strong NCW flux is documented within the high amplitude reflection band beneath horizon R5 (~12–10 Ma; Figs. 3–5; Müller-Michaelis et al., 2013). This strong NCW flux was also observed at Snorri, Bjorn, Gardar and Hatton Drifts between 13 and 10 Ma (Wold, 1994). We therefore suggest a deep current activity as depicted in Fig. 8c for the time interval 12–9 Ma. The shallowing of the deep circulation observed at Eirik Drift is reflected in circulation at shallower water depths of the northern North Atlantic Ocean, with drift building at Hatton Drift and the recirculation through the Irminger Sea (Fig. 8c). Bohrmann et al. (1990)

Fig. 7. Conceptual model for the development of palaeocurrents at Eirik Drift. Grey arrows indicate location and direction of the interpreted current core for the respective (sub)unit. Background morphology is that of each basal horizon for the sub-unit overlain by black-hatched depocentres of each sub-unit. Light grey lines show the location of the seismic profiles. Locations of mounds A, B and C are indicated by the white letters. Location of ODP Leg 105 Site 646 is marked by the yellow star. (a) Horizon A3 with depocentre and resulting palaeocurrent of seismic sub-unit SUIV-b (19–15 Ma); (b) horizon R5 with depocentre and resulting palaeocurrent of seismic sub-unit SUIV-a (12–8.1 Ma); (c) horizon R3/R4 with depocentre and resulting palaeocurrent of seismic sub-unit SUIII-b (7.5–5.6 Ma), the blue line indicates maximum eastern extent of top horizon R2; (d) horizon R2 (west of blue line) and R3/R4 (east of blue line) with depocentre and resulting palaeocurrent of seismic sub-unit SUIII-a (5.6–4.5 Ma), blue line indicates maximum eastern extent of bottom horizon R2; (e) horizon EU with depocentre and resulting palaeocurrent of seismic unit SUII (4.5–2.5 Ma); (f) horizon R1 with depocentre and resulting palaeocurrent of seismic sub-unit SUI-c (2.5–1.4 Ma); (g) horizon A2 with depocentre and resulting palaeocurrent of seismic sub-unit SUI-b (1.4–0.8 Ma); (h) horizon A1 with depocentre and resulting palaeocurrent of seismic sub-unit SUI-a (< 0.8 Ma).

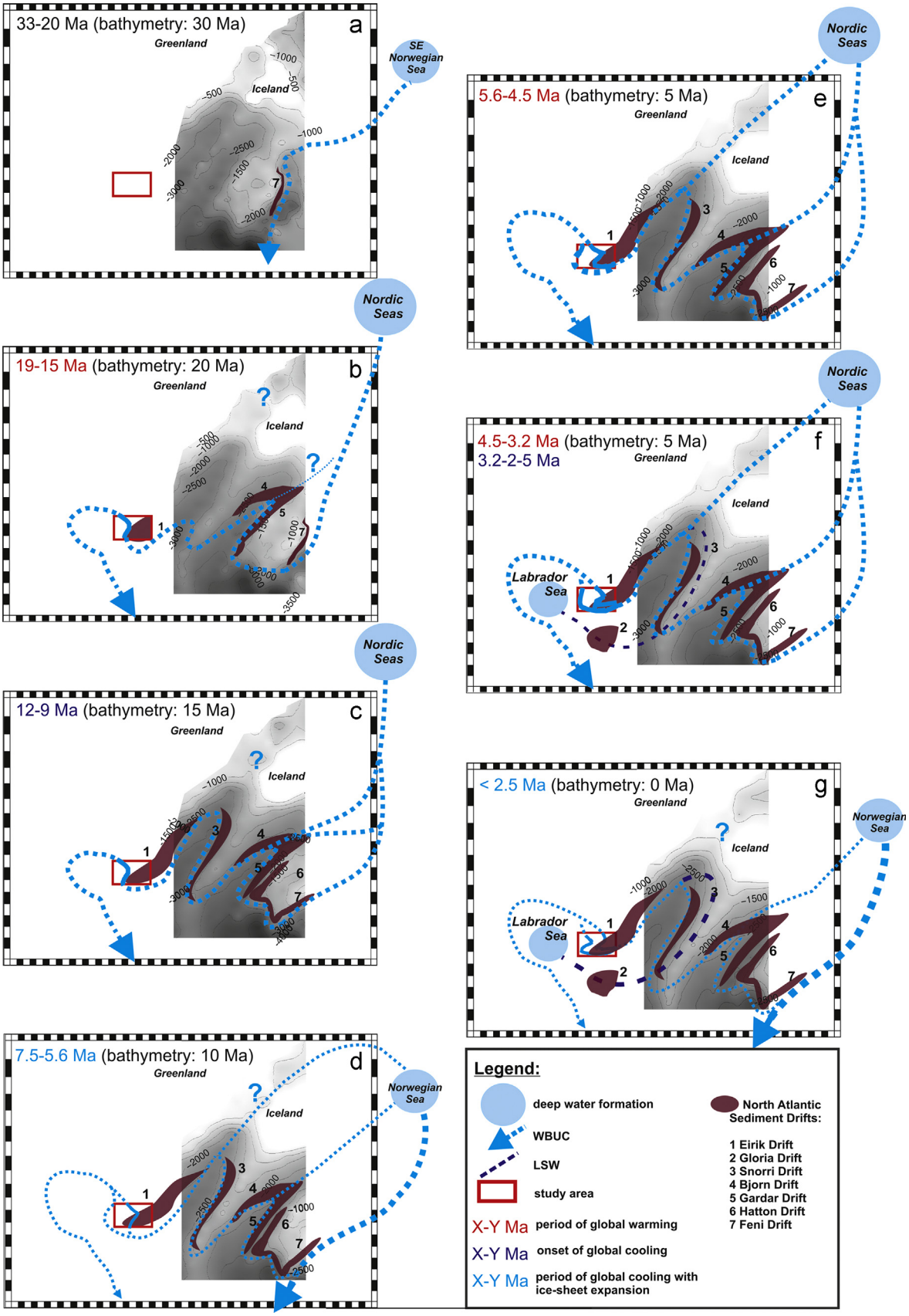

Fig. 8. Conceptual model for the deep palaeocirculation and location of NCW formation regions for the North Atlantic Ocean invoking our results from Eirik Drift. Palaeo-bathymetry after Ehlers and Jokat (2013). Location of the North Atlantic sediment drifts modified after Faugères et al. (1999). (a) 33–20 Ma, palaeo-bathymetry: 30 Ma. (b) 19–15 Ma, palaeo-bathymetry 20 Ma. (c) 12–9 Ma, palaeo-bathymetry 15 Ma. (d) 7.5–5.6 Ma, palaeo-bathymetry 10 Ma. (e) 5.6–4.5 Ma, palaeo-bathymetry 5 Ma. (f) 4.5–2.5 Ma, palaeo-bathymetry 5 Ma. (g) <2.5 Ma, palaeo-bathymetry 0 Ma.

reported of the first significant overflow over the western part of the Iceland–Scotland-Ridge at ~13–11 Ma (Fig. 8c). This strengthened the branch recirculating via the outer Labrador Sea supporting our interpretation of a shallower but intensified deep circulation after 12 Ma (Fig. 7b). The short-term (2–3 Ma) fluctuations in NCW flow after 12 Ma are suggested to be controlled by vertical motions of the GSR generated by the Icelandic mantle plume (Poore et al., 2006).

5.2. Unit SUIII (7.5–4.5 Ma)

The main depocentre of unit SUIII (~7.5–4.5 Ma) is found in the southwest of the study area, and additional smaller depocentres are found aligned along the western flanks of mounds A and B (Fig. 6d). In subunit SUIII-b the main depocentre is found S–N orientated west of mound C (Fig. 7c). The internal horizon R2 (~5.6 Ma), which marks the top of subunit SUIII-b, is only found in the west and onlaps the rise of horizon R3/R4 (Figs. 3 and 5). The main depocentre has shifted to the east and via a thin indention connects with the smaller depocentres aligned along the western flanks of mound A and B for subunit SUIII-a (Fig. 6d, Fig. 7c and d). The alongslope, S–N oriented depocentre in the west with parallel to subparallel internal reflections of low amplitudes is interpreted as a contourite deposit. The shape and orientation of subunit SUIII-b point to a northward directed NCW flow west of our study area for the period 7.5 to 5.6 Ma (Fig. 7c). With the shift of this depocentre to the E between 5.6 and 4.5 Ma we evidence this deeper, second branch of northward-directed flow with the observation of erosional centres in the NW of our study area (Fig. 3 (CDP < 400), Fig. 4 (CDP < 1000) and Fig. 7d). The locations of the onlap of the top horizon R2 (~5.6 Ma) onto horizon R3/R4 (7.5/8.1 Ma) can be interpreted as the erosional core of a shallower contour current branch, but no deposits are observed in the east (to the right of the erosional centres; Fig. 3 (CDP 3600), Fig. 4 (CDP 3600) and Fig. 7c). The onlap of horizon R2 (~5.6 Ma) onto horizon R3/R4 (7.5/8.1 Ma), i.e. the erosional deep current core centre, is observed within a distinct depth contour between ~4700 and 5300 ms TWT. The weak internal reflection amplitudes also point to a weak contour current as no lithological changes of the sediments were observed until 2.5 Ma (Cremer et al., 1989). It might have been too weak to transport sediments to the top of mounds A and B. Therefore, we suggest that the onlaps observed within the depth contour ~4700 to 5300 ms TWT mark the erosional centre of a shallower, weak contour current core even though no deposition is found to its right. The depositions along the western flanks of mounds A and B of subunit SUIII-a (~5.6–4.5 Ma) evidence this shallow NW directed flow (Fig. 3 (CDP 3800-6000), Fig. 6d and Fig. 7d). The part of the rms-defined depocentre where this suggested deep current core crosses is thin and just slightly exceeds the rms thickness value (Figs. 6 and 7d). The converging internal reflections at those locations in the seismic profiles (as an example Fig. 3 CDP 3000-4000) support the assumption of the crossing deep current core (Fig. 7d). The amplitudes of the internal reflections increase from the upper part of subunit SUIII-b towards the top of subunit SUIII-a (Figs. 3–5), where reflector truncations are observed at the erosional unconformity EU (insets Figs. 3–5). The enhanced erosional facies (reflector truncations) along with the increase in reflection amplitudes are interpreted as an increase in NCW flow with time following Stow et al. (2002), as no noteworthy changes in lithology were observed until 2.5 Ma (horizon R1) at ODP Site 646 (Cremer et al., 1989). The two branches of NCW flow observed after 5.6 Ma additionally flowed within a shallower depth contour (~4400–4800 ms TWT; Fig. 7d) than observed within subunit SUIII-b (~4700–5300 ms TWT; 7.5–5.6 Ma; Fig. 7c). Our data for the first time resolve the WSW flowing part at the SE flank of mound A via erosional centres with depocentres to their right (Fig. 3 (CDP > 7500), Fig. 4 (CDP > 5200), Fig. 5 (CDP < 1200) and Fig. 7d).

The first influence of NCW flow with an increased sedimentation rate at ODP Site 646 is reported at ~7.5 Ma (horizon R3) and was identified as DSOW (Kaminski et al., 1989). The onset of DSOW in the northern North Atlantic Ocean was also observed and dated ~7 Ma by Bohrmann et al. (1990) and followed the subsidence of the Denmark Strait due to the cooling of the Icelandic mantle plume at ~7 Ma (Poore et al., 2011). Thus, the depocentre overlying ODP Site 646 observed since 7.5 Ma might have been deposited under the influence of DSOW flow. We conclude that after 7.5 Ma the lower branch of the WBUC west of the study area transported (ancient) DSOW. Analogue to the modern deep current system we suggest that the upper observed branch conveyed Pre-ISOW. The observed weak NCW flow between 7.5 and 5.6 Ma have also been observed by Poore et al. (2006). Wright and Miller (1996) reported restricted overflows before ~6 Ma, and Arthur et al. (1989) also interpreted subunit SUIII-b to have formed under the influence of weak deep currents. Thus, the NCW flow at Eirik Drift and the northern North Atlantic Ocean is suggested to have been weak during the ongoing Miocene cooling (until ~6 Ma). Brackenridge et al. (2011) constituted weak NCW circulation by sea level lowstands during cold climate, which could be a hindering factor for exchange of deep-water masses at oceanic gateways, here the GSR. But still, high NCW production due to increased surface cooling could result in overflows as long as the sea level did not drop down to the gateway depth. Sea surface cooling and increase in salinity are preconditions of open ocean convection, which is the prevailing mechanism of NCW production and consequentially there should be increased NCW production and flow during cold phases. We suggest a significant ice cover of the Nordic Seas during this cold time interval. The ice cover would inhibit the open ocean convection as the ocean would be isolated from the atmosphere and no exchange in heat and freshwater would be possible. Unfortunately, only few details of the exact extent of sea ice are known for this period. A local glaciation at Svalbard is thought to have yielded a general strengthening of NHG at ~6.9 Ma (Winkler et al., 2002) and an enhanced sea-ice extent at the Greenland Sea between ~7.5 and 6.2 Ma (Wolf-Welling et al., 1996). The enhanced sea-ice extent would easily have resulted in a shift of the NCW formation area south towards the Norwegian Sea (Fig. 8d). With this southward shift, the pathways for the intense NCW branches would also have shifted, and therefore the Eirik and maybe also other Northwest Atlantic drifts experienced only a weaker branch of NCW flow. A denser, southward-directed NCW flow following a deeper depth contour is suggested as conveyor of the main deep circulation at that time (Fig. 8d). The only North Atlantic drift which documents intense deep-current velocities during cold climate stages is Feni Drift (Wold, 1994; Brackenridge et al., 2011), which supports our suggestion of a deep southward-directed NCW flow through the Rockall Trough region (Fig. 8d). The following intensification of NCW flow at Eirik Drift started with the climate reversal to the early Pliocene warm period (~5 Ma; Zachos et al., 2001). The onset of increasing deep current activity is documented at ODP Site 646 by an increase in deep ventilation at horizon R2 (5.6 Ma) (Kaminski et al., 1989) and here, highest deep current velocity is documented at the EU (4.5 Ma) (Kaminski et al., 1989). Increases in formation of ISOW are suggested at ~4.5 Ma (Haug and Tiedemann, 1998; Mikolajewicz and Crowley, 1997) and DSOW at ~4.6 Ma (Haug and Tiedemann, 1998). A distinct increase in drift accumulation at ~5 Ma is reported of at Bjorn and Gardar Drift (Wold, 1994). How can we explain this widespread observed intensification of the deep current system during the early Pliocene warm period? With the climate reversal and the warming, the suggested ice cover in the Greenland Sea was declined.

The deep-water formation region would then have shifted back to the Nordic Sea region including the Greenland Sea (Fig. 8e). With the climate warming a less dense and therefore shallower NCW flow is expected (Fig. 7d). We suggest that the main pathways of the NCW flow would then again have been similar to the present and therefore an intensification of the NCW flow along these pathways was observed (Fig. 8e).

5.3. Unit SUII (4.5–2.5 Ma)

For the period 4.5–2.5 Ma two connected depocentres are found shifted to the north while low to no deposition is found in the south and in the very east (Fig. 6f and Fig. 7e). The western part of the depocentre is found in the topographic low of the basal horizon EU at mound C, and the eastern part of the depocentre is found at the topographic high of the EU in the NE (Fig. 6e and f and Fig. 7e). In between these two parts the depocentre thins, and the internal reflection converge. Here, the rms-thickness value of 226 ms TWT is just slightly exceeded (Fig. 6f). Thinning and internal reflection characteristics of this indentation indicate that this part is more likely an erosional centre than part of the depocentre. Reflection truncations were found at horizon R1 at the eastern flank of mound A (Figs. 3–5 insets) and at the western flanks of mound B (Fig. 4) and mound C (Figs. 3 and 4). These distinct erosional centres again indicate an intense NCW flow of two branches in different depths. The locations of erosional and depositional centres as well as the morphology of the basal horizons suggest a WSW directed deep current flowing over the southern part of the study area and having been responsible for the low to non-deposition there (Fig. 6f and Fig. 7e). This NCW flow recirculated and split up into two northward-directed branches with the deeper branch accounting for the deposition at mound C (Fig. 7e). The upper branch overflowed the thinned indentation of the depocentre and deposits on top of mound A and B (Fig. 6f and Fig. 7e). Enhanced erosion and less sedimentation at the depth interval of the lower deep current branch indicate that the deeper part of NCW flow was more intense than the shallower branch (Fig. 6f and Fig. 7e). The pathways of the two deep current branches are similar to before. The similarity of pathways with enhanced erosion at the lower deep current branch might indicate that we again observe a strong NCW flow of DSOW (lower NCW) and ISOW (upper NCW), with a stronger DSOW than ISOW flow. Our interpretation of strong NCW flow from 4.5 to 2.5 Ma is supported by the findings of Arthur et al. (1989) at ODP Site 646. Poore et al. (2006) also reported strong NCW production between 5.2 and 2.7 Ma and Bohrmann et al. (1990) observed strong NCW flow between 4.8 and 3.2 Ma. Even though we interpret the NCW flow as strong, the two branches of the NCW flow shallowed and thus shifted upslope to the NE (Fig. 7d and e).

We again observe a strong NCW flow at Eirik Drift accompanied by a warm climate, the Pliocene warm period, which lasted until ~3.5 Ma (Ravelo, 2010; Zachos et al., 2001). We suggest Eirik Drift to still have lain within the main NCW flow produced in the complete Nordic Sea region. A major change to the period of unit SUIII is the observed shallowing of the deep current system (Fig. 8f). Following the closure of the Panama Isthmus (Burton et al., 1997) the formation of LSW commenced. The increase in northward deflection of warm and saline surface waters facilitated open ocean convection in the Labrador Sea (Via and Thomas, 2006). The onset of LSW flow is documented by the onset of drift building at the Gloria Drift at ~4.5 Ma (Wold, 1994; Fig. 8f). The entrainment of Labrador Sea Water (LSW) to both overflows, DSOW and ISOW, is supposed to have changed the density structure of the NCW and therefore yield a shallowed NCW flow at Eirik Drift (Fig. 7 e and Fig. 8f). The NCW flow remained strong during the transition to Pliocene cooling at ~3.2 Ma until 2.5 Ma.

5.4. Unit SUI (2.5–0 Ma)

In the following time intervals (2.5–1.4 Ma; 1.4–0.8 Ma; < 0.8 Ma) the depocentre in the north separated into two (Fig. 6h and Fig. 7f–h). The western depocentre infilled the eastern topographic low of the basal horizon and shifted southwards (Fig. 6h and Fig. 7f–h). The eastern depocentre remained on top of the topographic high of the basal horizon (Fig. 6h and Fig. 7f–h). Low deposition is observed in the south and surrounding the two depocentres, with less deposition found around the upper, eastern depocentre (Fig. 6h). Therefore, the suggested path of the deep current appeared to have remained almost unmodified with a gradual shift upslope (Fig. 7f–h), but with changes in intensity of the two branches. For 4.5–2.5 Ma we observed a higher intensity of the deeper flow (Fig. 6f and Fig. 7e) but now the stronger erosion is found at the upper branch (Fig. 6h and Fig. 7f–h), indicating a more intense upper NCW flow branch compared to the deeper. Converging reflections but no reflector truncations are observed at the NCW core locations (as examples Figs. 3–5), and therefore the erosion at the current core and thus the NCW flow is interpreted as less intense. The lack of reflector truncations indicates that the NCW flow not only shallowed but also weakened. Our interpretation is supported by Arthur et al. (1989), Kaminski et al. (1989) and Hunter et al. (2007b) who also observed a decrease in current intensity and an upslope migration of the drift crests at Eirik Drift after 2.5 Ma. A new thermal anomaly in the Icelandic mantle plume appeared at ~2.75 Ma and forced the GSR to uplift (Poore et al., 2011). This uplift might have restricted overflows at the Denmark Strait and only allowed deep-water exchange at the eastern part of the GSR (Fig. 8g). The observed shallowing and weakening of the NCW flow system at Eirik Drift is accompanied by Pliocene cooling with intensification of Northern Hemisphere Glaciation (NHG). The NHG intensification is documented at ODP Site 646 via horizon R1 (2.5 Ma) with the onset of ice-rafting (Arthur et al., 1989; Cremer et al., 1989). Pronounced ice-sheet expansion in the Northern Hemisphere is reported for 2.75 Ma (Ravelo, 2010) and 2.6 Ma (Bohrmann et al., 1990; Wolf-Welling et al., 1996).

We propose that the sea ice cover of the Nordic Seas again shifted the NCW formation regions towards the south and that Eirik Drift only experienced the influence of weaker branch of the NCW circulation. The main part of NCW flow is suggested to have been dense and to have flowed at deeper depth contours directly towards the south and not overflowing the uplifted Denmark Strait (Fig. 8g). With an enhanced ice extent not only covering the Greenland Sea but also the northern part of the Norwegian Sea, the NCW formation region would have been shifted to the SE Norwegian Sea. In that case, the leakage via the uplifted Denmark Strait might have stopped and the two branches observed of NCW flow observed at Eirik Drift comprised ISOW (lower NCW) and LSW (upper NCW). It is also possible that there still was a leakage of DSOW and that the shallowing of the DSOW and ISOW branches was caused by an increased entrainment of LSW, which would have changed the density structure of the overflows. During cold phases increased deep-water formation would have taken place in the Labrador Sea. The distinct drift growths at the Gloria and Snorri Drifts during this time interval (Wold, 1994) and also the enhanced erosion of the upper branch compared to the lower branch at Eirik Drift is suggested to have been forced by an enhanced LSW circulation or entrainment, respectively, during this time interval. Besides the growth of Gloria and Snorri Drifts due to intensified LSW flow, only Feni Drift recorded an intense deep current activity in the northern North Atlantic Ocean (Wold, 1994). At Feni Drift the most vigorous deep-water velocity is documented during glacials and the influencing water masses are of Norwegian Sea and Southern Ocean origin. However, Hatton

Drift underwent intense NCW flow during interglacials (Brackenridge et al., 2011). This combination supports our assumption of a deep, intense, southward-directed NCW flow originating in the Norwegian Sea, which did not recirculate through the basins west of Rockall Trough.

6. Summary and conclusion

A detailed conceptual model for the palaeocirculation at Eirik Drift was developed by analysing the morphology of prominent horizons and the location and orientation of erosional and depositional centres (Fig. 7). The local changes derived for Eirik Drift were linked to changes in North Atlantic climate (Fig. 8). Summing up our investigations, for Eirik Drift we suggest strong NCW flow during warm climates and at the beginning of cooling phases and weak NCW flow during enhanced cooling phases accompanied by NHG. This interpretation is in concordance with studies on many other NA drifts. Since open ocean convection is the prevailing mechanism for the present deep-water formation in the Nordic Seas (Van Aken, 2007) and open ocean convection is dependent on ocean–atmosphere interplay of surface cooling and enhanced salt input to the oceans surface, we would expect increased NCW formation and flow during cold climate conditions when atmospheric cooling is highest and much freshwater is bound in land and sea ice. However, during times of NHG the Nordic Sea basins were partly covered with ice, which inhibits ocean–atmosphere exchanges. Therefore, we conclude that the NCW formation regions shifted southwards to the Norwegian Sea during phases with enhanced ice cover over the Nordic Seas and that the main NCW flow during these cold phases did not affect Eirik Drift. We suggest a dense, deep southward-directed NCW flow through Rockall Trough during these cold phases, whilst the residual northern North Atlantic Ocean was just affected by weaker branches of the deep circulation system. During warmer phases, when the Nordic Seas showed a significant smaller ice cover, the NCW formation regions shifted back north and the flow pattern was more similar to the modern one with overflows over the GSR and a main NCW flow recirculating via the outer Labrador Sea (Eirik Drift). Therefore, the NCW flow is observed intensified at Eirik Drift region during warm phases and at the beginning of cooling with no observed ice cover of the Nordic Sea region and weakened during cool climate with enhanced ice extent. Our suggested conceptual model for the palaeocirculation is summarized as follows:

1. Eirik Drift area was characterized by a tranquil environment until ~19 Ma (Müller-Michaelis et al., 2013). Strong NCW flow at Eirik Drift is suggested between 19 and 15 Ma (Müller-Michaelis et al., 2013) during Miocene warming (Fig. 8b). NCW overflow was inhibited between ~15 and 12.5 Ma (Müller-Michaelis et al., 2013) following the Mid Miocene Climatic Optimum. A renewed onset of strong NCW flow is inferred between 12 and 9 Ma (Müller-Michaelis et al., 2013) following the Miocene transition to a colder climate and the subsidence of the GSR (Fig. 8c). NCW flow in this time period is suggested to consist of ISOW, as Denmark Strait was still too shallow to allow deep-water overflow (Fig. 8a–c).
2. We suggest a weak WBUC for the period 7.5–5.6 Ma during Miocene cooling (~13–6 Ma). The Miocene cooling may have yield an enhanced ice cover of the Greenland Sea between ~7.5 and 6.2 Ma and thus, the NCW formation region is suggested to have shifted towards the Norwegian Sea. The main NCW dispersal route is suggested to have run south through the Rockall Trough as intense NCW flow is documented only in Feni Drift (Wold, 1994; Brackenridge et al., 2011) (Fig. 8d). For the first time the separation of NCW flow into two branches in two different water depths is observed. These are interpreted to represent weak branches of NCW, DSOW (lower NCW) and ISOW (upper NCW) (Fig. 8d).
3. An intense NCW flow is inferred during the early Pliocene warm period and the beginning of Pliocene cooling between 5.6 and 2.5 Ma (Fig. 8e). We suggest that the NCW formation region and NCW flow paths shifted back to similar locations like at present and Eirik Drift lay under the main NCW dispersal route. The NCW flow system shallowed after 4.5 Ma, presumably due to the influence of entrained LSW on the density structure of the overflows (Fig. 8f).
4. With the intensification of NHG a weakening of the deep current system is inferred after 2.5 Ma (Fig. 8g). The NCW formation region is suggested to have shifted to the SE Norwegian Sea due to ice coverage of the Greenland Sea and northern Norwegian Sea. The main NCW flow again is suggested to have flown south through Rockall Trough towards the eastern North Atlantic Ocean as solely Feni Drift documents intense NCW flow during glacials (Wold, 1994; Brackenridge et al., 2011). The weaker, shallower branches of NCW flow, which affected Eirik Drift, might have transported ISOW (lower NCW) and LSW (upper NCW) if DSOW was restricted or DSOW (lower NCW) and ISOW (upper NCW) with larger portions of entrained LSW.

Our investigation helped to shed more light on the complex interplay of changes in ocean currents, climate and tectonics in the northern North Atlantic Ocean. Still, further details are needed to decipher the whole complex system. More high-resolution seismic lines covering a larger study area as well as additional deep drilling at mound A to gather ground truth information are needed to advance our knowledge.

Acknowledgements

We are grateful for the support of Captain F. von Staa, his officers and crew during RV Maria S. Merian cruise MSM 12/2. The data collection was funded within the core program METEOR/MERIAN provided by the Deutsche Forschungsgemeinschaft (DFG). This work was funded by the DFG under grant no. Ue 49/12. We extend thanks to Dr. M.P. Bacon (editor) and four anonymous reviewers for their comments, which improved our manuscript.

References

Arthur, M.A., Srivastava, S.P., Kaminski, M., Jarrard, R.D., Osler, J., 1989. Seismic stratigraphy and history of deep circulation and sediment drift development in Baffin Bay and the Labrador Sea. In: Srivastava, S.P., Arthur, M., Clement, B., et al. (Eds.), Proceedings of the Ocean Drilling Program, Scientific Results, vol. 105, College Station, TX, pp. 957–988.

Bohrmann, G., Henrich, R., Thiede, J., 1990. Miocene to Quaternary paleoceanography in the northern North Atlantic: variability in carbonate and biogenic opal accumulation. In: Bleil, U., Thiede, J. (Eds.), Geological History of the Polar Oceans: Arctic Versus Antarctic, 308. Springer, Netherlands, pp. 647–675.

Brackenridge, R., Stow, D.A.V., Hernández-Molina, F.J., 2011. Contourites within a deep-water sequence stratigraphic framework. Geo-Mar. Lett. 31, 343–360.

Burton, K.W., Ling, H.-F., O'Nions, R.K., 1997. Closure of the Central American Isthmus and its effect on deep-water formation in the North Atlantic. Nature 386, 382–385.

Chalmers, J.A., Pulvertaft, T.C.R., 2001. Development of the continental margins of the Labrador Sea—a review. In: Wilson, R.C.L., Whitmarsh, R.B., Froitzheim, N. (Eds.), Non-volcanic Rifting of the Continental Margins: A Comparison of Evidence from Land and Sea. Geological Society, London, pp. 77–105.

Channell, J.E.T., Sato, T., Kanamatsu, T., Stein, R., Alvarez Zarikian, C.A., 2010. Expedition 303/306 synthesis: North Atlantic climate. In: Channell, J.E.T., Kanamatsu, T., Sato, T., Stein, R., Alvarez Zarikian, C.A., Malone, M.J., and the Expedition 303/306 Scientists. (Eds.), Proceedings of the Integrated Ocean Drilling Program, vol. 303/306, College Station, TX.

Cremer, M., Maillet, N., Latouche, C., 1989. Analysis of sedimentary facies and clay mineralogy of the Neogene-Quaternary sediments in ODP Site 646, Labrador Sea. In: Srivastava, S.P., Arthur, M., Clement, B. (Eds.), Proceedings of the Ocean Drilling Program, Scientific Results, vol. 105, College Station, TX, pp. 71–80.

Davies, R., Cartright, J., Pike, J., Line, C., 2001. Early Oligocene initiation of North Atlantic Deep Water formation. Nature 410, 917–920.

Dickson, R.R., Brown, J., 1994. The production of North Atlantic Deep Water: sources, rates, and pathways. J. Geophys. Res. 99 (C6), 12319–12341.

Ehlers, B.-M., Jokat, W., 2013. Paleo-bathymetry of the northern North Atlantic and consequences for the opening of the Fram Strait. Mar. Geophys. Res. , http://dx.doi.org/10.1007/s11001-013-9165-9.

Faugères, J.C., Stow, D.A.V., 2008. Contourite drifts: nature, evolution and controls. In: Rebesco, M., Camerlenghi, A. (Eds.), Contourites. Elsevier, Netherlands, pp. 259–288.

Faugères, J.C., Stow, D.A.V., Imbert, P., Viana, A.R., 1999. Seismic features diagnostic of contourite drifts. Mar. Geol. 162, 1–38.

Haug, G.H., Tiedemann, R., 1998. Effect of the formation of the Isthmus of Panama on Atlantic Ocean thermohaline circulation. Nature 393, 673–676.

Heezen, B.C., Hollister, C.D., Ruddiman, W.F., 1966. Shaping the continental rise by deep geostrophic contour currents. Science 152, 502–508.

Hunter, S., Wilkinson, D., Louarn, E., McCave, I.N., Rohling, E., Stow, D.A.V., Bacon, S., 2007a. Deep western boundary current dynamics and associated sedimentation on the Eirik Drift, Southern Greenland Margin. Deep Sea Res. Part I 54, 2036–2066.

Hunter, S., Wilkinson, D., Stanford, J., Stow, D.A.V., Bacon, S., Akhmetzhanov, A.M., Kenyon, N.H., 2007b. The Eirik Drift: a long-term barometer of North Atlantic deepwater flux south of Cape Farewell, Greenland. In: Viana, A.R., Rebesco, M. (Eds.), Economic and Palaeoceanographic Significance of Contourite Deposits, vol. 276. Geological Society, Special Publications, London, pp. 245–263.

Kaminski, M.A., Gradstein, F.M., Scott, D.B., Mackinnon, K.D., 1989. Neogene benthic foraminifer biostratigraphy and deep-water history of Sites 645, 646, and 647, Baffin Bay and Labrador Sea. In: Srivastava, S.P., Arthur, M., Clement, B., et al. (Eds.), Proceedings of the Ocean Drilling Program, Scientific Results, vol. 105, College Station, TX, pp. 731–756.

Kuhlbrodt, T., Griesel, A., Montoya, M., Levermann, A., Hofmann, M., Rahmstorf, S., 2007. On the driving processes of the Atlantic meridional overturning circulation. Rev. Geophys. 45 (2), RG2001.

Le Pichon, X., Hyndman, R.D., Pautot, G., 1971. Geophysical study of the opening of the Labrador Sea. J. Geophys. Res. 76 (20), 4724–4743.

Marshall, J., Speer, K., 2012. Closure of the meridional overturning circulation through Southern Ocean upwelling. Nat. Geosci. 5, 171–180.

Mikolajewicz, U., Crowley, T.J., 1997. Response of a coupled ocean/energy balance model to restricted flow through the central American isthmus. Paleoceanography 12 (3), 429–441.

Miller, K.G., Tucholke, B.E., 1983. Development of Cenozoic abyssal circulation south of the Greenland–Scotland Ridge. In: Bott, M.H.P., Saxov, S., Talwani, M., Thiede, J. (Eds.), Structures and Development of the Greenland–Scotland Ridge—New Methods and Concepts. Plenum Press, New York and London, pp. 549–589.

Miller, K.G., Wright, J.D., Katz, M.E., Wade, B.S., Browning, J.V., Cramer, B.S., Rosenthal, Y., 2009. Climate threshold at the Eocene–Oligocene transition: Antarctic ice sheet influence on ocean circulation. In: Koeberl, C., Montanari, A. (Eds.), The Late Eocene Earth-Hothouse, Icehouse, and Impacts, 452. Geological Society of America Special Paper, pp. 169–178.

Müller-Michaelis, A., Uenzelmann-Neben, G., Stein, R., 2013. A revised Early Miocene age for the instigation of the Eirik Drift, offshore southern Greenland: evidence from high-resolution seismic reflection data. Mar. Geol., 340. http://dx.doi.org/10.1016/j.margeo.2013.04.012.

Nielsen, T., Knutz, P.C., Kuijpers, A., 2008. Seismic expression of contourite depositional systems. In: Rebesco, M., Camerlanghi, A. (Eds.), Contourites. Elsevier, Netherlands, pp. 301–321.

Pickart, R.S., 1992. Water mass components of the North Atlantic deep western boundary current. Deep Sea Res. 39, 1553–1572.

Poore, H.R., Samworth, R., White, N.J., Jones, S.M., McCave, I.N., 2006. Neogene overflow of Northern Component Water at the Greenland–Scotland Ridge. Geochem. Geophys. Geosyst. 7 (6), Q06010.

Poore, H., White, N., MacLennan, J., 2011. Ocean circulation and mantle melting controlled by radial flow of hot pulses in the Iceland plume. Nat. Geosci. 4 (8), 558–561.

Quadfasel, D., Käse, R., 2007. Present-day manifestation of the Nordic Seas Overflows. In: Schmittner, A., Chiang, J.C.H., Hemming, S.R. (Eds.), Ocean Circulation: Mechanisms and Impacts—Past and Future Changes of Meridional Overturning. American Geophysical Union, Washington, DC, pp. 75–89.

Ravelo, A.C., 2010. Palaeoclimate: warmth and glaciation. Nat. Geosci. 3 (10), 672–674.

Schmitz Jr., W.J., 1996. On the World Ocean Circulation. Volume I, Some Global Feature/North Atlantic Circulation (Technical Report WHOI-96-03). Woods Hole Oceanographic Institution, Woods Hole, MA.

Shipboard Scientific Party, 1987. Site 646. In: Srivastava, S.P., Arthur, M., Clement, B., et al. (Eds.), Initial Reports 105. Ocean Drilling Program, College Station, TX, pp. 419–674.

Smethie, W.R.J., Fine, R.A., 2001. Rates of North Atlantic Deep Water formation calculated from chlorofluorcarbon inventories. Deep Sea Res. Part I 48, 189–215.

Smith, W.H.S., Sandwell, D.T., 1997. Global sea floor topography from satellite altimetry and ship depth soundings. Science 277, 1956–1962.

Srivastava, S.P., Arthur, M.A., 1989. Tectonic evolution of the Labrador Sea and Baffin Bay: constraints imposed by regional Geophysics and drilling results from Leg 105. In: Srivastava, S.P., Arthur, M., Clement, B., et al. (Eds.), Proceedings of the Ocean Drilling Program, Scientific Results, vol. 105, College Station, TX, pp. 989–1009.

Srivastava, S.P., Roest, W.R., 1999. Extent of oceanic crust in the Labrador Sea. Mar. Pet. Geol. 16 (1), 65–84.

Stoker, M.S., Hoult, R.J., Nielsen, T., Hjelstuen, B.O., Laberg, J.S., Shannon, P.M., Praeg, D., Mathiesen, A., van Weering, T.C.E., McDonnell, A., 2005. Sedimentary and oceanographic responses to early Neogene compression on the NW European margin. Mar. Pet. Geol. 22 (9–10), 1031–1044.

Stow, D.A.V., Faugères, J.-C., Howe, J.A., Pudsey, C.J., Viana, A.R., 2002. Bottom currents, contourites and deep-sea sediment drifts: current state-of-the-art. In: Stow, D.A.V., Pudsey, C.J., Howe, J.A., Faugères, J.-C., Viana, A.R. (Eds.), Deep-water Contourite Systems: Modern Drifts and Ancient Series, 22. Geological Society of London, London, pp. 7–20.

Stow, D.A.V., Hunter, S., Wilkinson, D., Hernández-Molina, F.J., 2008. The nature of contourite deposition. In: Rebesco, M., Camerlenghi, A. (Eds.), Contourites. Elsevier, Netherlands, pp. 143–156.

Uenzelmann-Neben, G., 2001. Seismic characteristics of sediment drifts: an example from the Agulhas Plateau, southwest Indian Ocean. Mar. Geophys. Res. 22, 323–343.

Uenzelmann-Neben, G., Gohl, K., 2012. Amundsen Sea sediment drifts: Atchives of modifications in oceanographic and climatic conditions. Mar. Geol. 229–302, 51–62.

Uenzelmann-Neben, G., Huhn, K., 2009. Sedimentary deposits on the South African continental margin: slumping versus non-deposition or erosion by oceanic currents? Mar. Geol. 266 (1–4), 65–79.

Uenzelmann-Neben, G., Schlüter, P., Weigelt, E., 2007. Cenozoic oceanic circulation within the South African gateway: indications from seismic stratigraphy. S. Afr. J. Geol. 110 (2–3), 275–294.

Uenzelmann-Neben, G., Schmidt, D.N., Niessen, F., Stein, R., 2012. Intraplate volcanism off South Greenland caused by glacial rebound? Geophys. J. Int. 190 (1), 1–7.

Van Aken, H.M., 2007. The Oceanic Thermohaline Circulation. Springer, New York.

van Weering, T., Stoker, M., Rebesco, M., 2008. High-latitude contourites. In: Rebesco, A., Camerlenghi, A. (Eds.), Contourites. Elsevier, Netherlands, pp. 457–489.

Via, R.K., Thomas, D.J., 2006. Evolution of Atlantic thermohaline circulation: early Oligocene onset of deep-water production in the North Atlantic. Geology 34, 441–444.

Winkler, A., Wolf-Welling, T., Stattegger, K., Thiede, J., 2002. Clay mineral sedimentation in high northern latitude deep-sea basins since the Middle Miocene (ODP Leg 151, NAAG). Int. J. Earth Sci. 91 (1), 133–148.

Wold, C.N., 1994. Cenozoic sediment accumulation on drifts in the northern North Atlantic. Paleoceanography 9 (6), 917–941.

Wolf-Welling, T.C.W., Cremer, M., O'Connell, S., Winkler, A., Thiede, J., 1996. Cenozonic Arctic gateway paleoclimate variability: indications from changes in coarse-fraction compositions. In: Thiede, J., Myhre, A.M., Firth, J.V., Johnson, G.L., Ruddiman, W.F. (Eds.), Proceedings of the Ocean Drilling Program—Scientific Results, vol. 151, College Station, TX, pp. 515–567.

Woodruff, F., Savin, S., 1989. Miocene deepwater oceanography. Palaeogeography 4, 87–140.

Wright, J.D., 1998. Role of the Greenland–Scotland Ridge in Neogene climate changes. In: Crowley, T.J., Burke, K. (Eds.), Tectonic Boundary Conditions for Climate Reconstructions. Oxford University Press, Oxford, pp. 192–211.

Wright, J.D., Miller, K.G., 1996. Control of North Atlantic Deep Water circulation by the Greenland–Scotland Ridge. Paleoceanography 11 (2), 157–170.

Wright, J.D., Miller, K.G., Fairbanks, R.G., 1992. Early and middle Miocene stable isotopes: implications for deepwater circulation and climate. Paleoceanography 7, 357–389.

Zachos, J.C., Pagani, M., Sloan, L., Thomas, E., Billups, K., 2001. Trends, rhythms, and aberrations in global climate 65 Ma to present. Science 292, 686–693.